RSC Advances

ROYAL SOCIETY OF CHEMISTRY

www.rsc.org/advances

RSC Advances

ARTICLE

The preparation of TiO_2 composite materials modified with Ce and tourmaline and their photocatalytic activity study

Received 00th January 20xx,
Accepted 00th January 20xx

DOI: 10.1039/x0xx00000x

www.rsc.org/

Hong Zhang,[abc] Aiju Lv, [abc] Jinsheng Liang[†abc] and Junping Meng[abc]

Rare earth cerium (Ce), borosilicate mineral tourmaline and titanium dioxide (TiO_2) composite photocatalysts were prepared via a sol-gel method. Through detecting the microstructure and the methyl orange (MO) photocatalytic activity of the composite photocatalysts with different preparation processes and component contents, this paper has discussed the effects of tourmaline and Ce on the composite catalysts about the preparation and photocatalytic activity. Among different composite photocatalysts, the sample with the following addition sequence and proportions possessed the highest MO degradation ratio in 3 h (94.6%): 0.10 wt% of Ce was added into the primary alkoxide solution and 0.40 wt% of tourmaline addition after the titanium sol, which synergy effected on the microstructure of photocatalyst nanoparticles wrapped around fine tourmaline particles during preparation and the high activity to photodegradate organic pollutants in water.

Introduction

Due to the advantages of inexpensive preparation, innocuity, high efficiency and strong oxidizing power, titanium dioxide (TiO_2) photocatalyst has shown broad application prospect in the field of photodegrading organics for pullutant treatment, water decontamination and antibacterial environmental, which has attracted much attention in the last decade as considered the green and most promising environmental protection material [1,2]. In terms of the TiO_2 preparation, various chemical and physical treatment techniques have been investigated, such as sol-gel method, hydrothemeral method, chemical vapor deposition method and so on [3-5]. Despite its fascinating properties, TiO_2 has a wide band gap of 3.2 eV and a high recombination rate of the photogenerated electron-hole pair. Thus, the low solar energy utilization rate (the ultraviolet portion with the wavelength of less than 387.5 nm) and quantum efficiency, resulted in limiting the industrial application of TiO_2 prepared by traditional methods [3]. Therefore, TiO_2 must be modified to narrow down the band gap and hinder the recombination of photogenerated electron-hole, for enhancing the light availability and photocatalytic activity [6,7]. TiO_2 modified with metal nanoparticles is effective to obtain more efficient photocatalytic activity. Zhang *et al.* [8] have modified TiO_2 with four kinds of noble metal (Pt, Rh, Pd, Au) synthesis composite materials respectively. By observing the effect on the photocatalitic degradation of formaldehyde, the author found the best load is 1%Pt/TiO_2. However, noble metals are too expensive to apply practically. Moreover, some workers have employed effective non-precious transition metals to modify TiO_2, which could make the band gap narrow, and produce more photogenerated electron-hole, so that enhance the redox ability of TiO_2 [9-12]. Recently, it has been reported that the incorporation of lanthanide ions or oxides into TiO_2 resulted in highly efficient photocatalytic activity due to their special f and d electron orbital structure [13-15]. Among these ions, cerium (Ce) produced much more effective photocatalytic activity when being doped TiO_2 [16-20].

In addition, researchers have utilized the electrostatic poles of tourmaline crystals to improve TiO_2 photocatalysis in recent years [21-25]. Tourmaline is a complex borosilicate mineral, belonging to the trigonal space group, has the spontaneous and permanent polarity, which can produce an electric dipole. The general chemical formula of tourmaline can be written as $XY_3Z_6Si_6O_{18}(BO_3)_3W_4$ (where X is Na^+, Ca^{2+}, K^+ or vacancies; Y is Mg^{2+}, Mn^{2+}, Fe^{2+}, Al^{3+}, Fe^{3+}, Mn^{3+} or Li^+; Z is Al^{3+}, Fe^{3+}, Cr^{3+} or Mg^{2+}; W is OH^-, F^-, O^{2-})[26,27]. As heteropolar mineral, the three fold symmetry axis of tourmaline is the C axis, and there is neither axis nor center of symmetry perpendicularly to the C axis. The unique elements and structure make tourmaline feature many important properties such as piezoelectricity, pyroelectricity, irradiating far infrared, and a strong electric field existing on the surface of a tourmaline granule, like an electric dipole, especially in a small granule with a diameter of microns or less. Liang *et al.* [21] prepared tourmaline/TiO_2 composite films by sol-gel method, to modify TiO_2 by forming

[a] Key Laboratory of Special Functional Materials for Ecological Environment and Information (Hebei University of Technology), Ministry of Education, Tianjin 300130, People's Republic of China.
[b] Institute of Power Source and Ecomaterials Science, Hebei University of Technology, Tianjin 300130, People's Republic of China.
[c] Key Laboratory for New Type of Functional Materials in Hebei Province, Hebei University of Technology, Tianjin 300130, People's Republic of China.
†Corresponding Author
Fax/Tel: +86 22 60204850; E-mail: liangjinsheng@hebut.edu.cn
See DOI: 10.1039/x0xx00000x

different microstructure through adding tourmaline and changing preparation method, and it was found photocatalytic activity of TiO_2 was effectively enhanced.

In view of the strong electric field and high far-infrared radiation of natural tourmaline, and unique characteristics of rare earth elements, we propose the application of sol-gel technology to prepare nanometer TiO_2 composite materials with trace rare earth Ce and tourmaline. Though evaluating the photocatalytic degradation of methyl orange (MO), the aim of our study is to explore the synergistic-effect of Ce and tourmaline on the TiO_2 composite materials, including the impact about the addition sequence and content of Ce and tourmaline on the microstructure of TiO_2 composite photocatalysts, and the ultimate enhance of their photocatalytic activity. It is expected to provide a green and promising engineering to improve the organic pollutants degradation for protecting environment.

Experimental

2.1 Photocatalysts

TiO_2 and different TiO_2 composite photocatalysts with Ce or tourmaline were prepared as follow (the preparation process and component proportion of Sample A-F were list in Table 1):

As the control sample TiO_2 sol, the primary alkoxide solution was prepared with $Ti(OC_4H_9)_4$ dissolved in C_2H_5OH (1:5, mass ratio) and marked as (a). HCl, CH_3COOH and deionized water (16.180 g, 7.4 mL and 1.3 mL, respectively, marked as (b)) were mixed with this solution (pH=2.0). After stirring for 3 h, the resultant alkoxide solution was kept at room temperature for 2 h of hydrolysis reaction.

For different TiO_2 composite photocatalysts, the blending aqueous solution, including cerous nitrate (0.008 g of $Ce(NO_3)_3{\cdot}6H_2O$) and ethanol (65 mL), was marked as (c); the tourmaline suspension with ethanol (0.010 g of tourmaline, 65 mL of ethanol), was marked as (t). The (c) or (t) solution, or both of the two solution were added dropwise following the different sequences (Preparation process of Table 1), and were stirred for 3 h. The tourmaline particles used here were black tourmaline from Hebei Province, China. The particle size of the black tourmaline (D_{50}) was 0.40 μm. The main chemical compositions of tourmaline were as follow (wt%, dry mass): Al_2O_3 35.98; B_2O_3 10.94; K_2O 0.04; Na_2O 0.91; MgO 0.20; SiO_2 34.60; Fe_2O_3 15.80; CaO trace. In the experiment, $Ti(OC_4H_9)_4$, CH_3COOH, HCl and other chemicals used were analytical reagent.

The stainless steel meshes were used as substrates for thin films. Before preparation, the stainless steel meshes (100 mm × 100 mm) were subjected to pre-treatment, which was as follows. The stainless steel meshes were washed by acid and rinsed by deionized water and ethanol, respectively. Finally, the meshes were well prepared after drying. The photocatalyst films were prepared with the above sol solutions by dipping-withdrawing on stainless steel meshes in ambient atmosphere. The meshes were firstly dipped into the sol for 10 min. The withdrawal speed was 50 mm/min. The substrates coated with gel films were dried naturally for 1 h, and subsequently heat-treated at 600 ℃ for 2 h. All the photocatalyst film samples were thus prepared and the ultimate component proportion of different photocatalyst samples were calculated as shown in Table 1.

2.2 Characterization

200 mL deionized water was injected into a plastic bottle, which was wrapped with a 4 mm-thick circle layer of tourmaline particles outside. The electrical conductivity and surface tention of deioned water were observed three times interval 30 min by digital conductivity meter (DDS-11AT, China) and automatic tensiometer (JK99B, China), respectively.

Different Sample A-F films on stainless steel meshes were scraped, and these sample powders were collected. For the crystal structure of the photocatalyst samples, the powders of Sample A-F were characterized via X-ray diffraction (XRD, Philips-X, Pert MPD, Holland) with Cu Kα radiation (λ= 0.1540 nm).

The different photocatalyst powders were determined by energy dispersive spectroscopy (EDS) analysis, and the

Table 1 The process parameters and component proportion of different photocatalyst samples

Samples	Amount of compositions			Preparation process	Component proportion of the ultimate (wt%)		
	$Ti(OC_4H_9)_4$ (g)	$Ce(NO_3)_3{\cdot}6H_2O$ (g)	Tourmaline (g)		TiO_2	Ce	Tourmaline
A	11.000	-	-	(a)+(b)	100	-	-
B	10.623	0.008	-	(a)+(c)+(b)	99.9	0.1	-
C	10.594	-	0.010	(a)+(b)+(t)	99.6	-	0.4
D	10.583	0.008	0.010	(a)+(c)+(t)+(b)	99.5	0.1	0.4
E	10.583	0.008	0.010	(a)+(b)+(c)+(t)	99.5	0.1	0.4
F	10.583	0.008	0.010	(a)+(c)+(b)+(t)	99.5	0.1	0.4

(a)The primary alkoxide solution ($Ti(OC_4H_9)_4$:C_2H_5OH=1:5, mass ratio)

(b)HCl and CH_3COOH solution

(c)The cerous nitrate solution with ethanol

(t) The tourmaline suspension with ethanol

microstructures of different sample films were observed by scanning electron microscope (SEM, Hitachi, S-4800, Japan) and transmission electron microscopy (TEM, JEOL JEM-100CX Ⅱ, Japan). The Brunauer-Emmett-Teller (BET) surface area was determined by nitrogen adsorption measurement at 77K (Quantachrome, Autosorb-iQ, USA).

The absorption edge of different samples was measured by ultraviolet (UV)-vis diffuse reflectance spectra (UV-vis Spectrophotometer, Hitachi, U-3900H, Japan) and $BaSO_4$ was used as a reflectance standard.

The photocatalytic activity of different film samples were evaluated by MO degradation. An UV lamp (25 W, 253.7 nm) was used as a light source, with a 40 cm-distance to the bottom of the reactor, and the averaged intensity of UV irradiance was 49 mW/cm^2. For MO photodegradation, sample films (100 mm × 100 mm) were put into the bottom of the reactor, with pure quartz glass sealed on the top. 100 mL aqueous solution of MO (20 mg/L) were dropped into the reactor, the effective depth of reaction liquid is about 9.6 mm. The changes of MO concentration were detected by UV-vis spectrophotometer (UV-vis, TU-1810PC, China) interval 20 min. During MO photodegradation, the pH values of every sample reaction were detected by pH meter (Leici, PHS-3E, China) at 0 h, 1 h, 2 h and 3h. The optical images of MO photodegradation by Sample A-F were also taken at different time (0 h and 3 h).

For investigating the generation of OH radicals by phothocatalysts, a stock terephthalic acid solution (with 5×10^{-4} M terephthalic acid and 2×10^{-3} M NaOH) was prepared to as described in the literatures [28-30]. Sample A-F was added into the stock solution, respectively. The suspensions were irradiated by the UV lamp for 30 min, collected and centrifugated for PL measurements. Fluorescence spectra were measured on fluorescence spectrophotometer (Hitachi, F-4500, Japan) with an excitation wavelength of 320nm.

For discussion the effect on photocatalytic activity of TiO_2 composite film, different component proportions of tourmaline and Ce in Sample F were studied.

Results and discussion

3.1 The electrical conductivity and surface tension of deionized water with tourmaline

Table 2 showed the differences about electrical conductivity and surface tension of deionized water wrapped with or without tourmaline. The electrical conductivity of deionized water was kept around 1.58 μs/cm (without tourmaline), and increased to 2.07 μs/cm with the time of being wrapped around tourmaline for 120 min. The surface tension of deionized water was about 72 mN/m (without tourmaline), and reduced to 65 mN/m approximately (with tourmaline). The deionized water was wrapped with tourmaline particles outside plastic bottle, therefore the electric field of tourmaline would not affect the electrical conductivity and surface tension of deionized water. Moreover, the high far-infrared radiation of tourmaline particles could penetrate through the plastic bottle, provide energy to enhance molecular vibration and diminish the clusters of water molecules.

The high far-infrared radiation of tourmaline is due to the infrared activity of vibration in its crystal structure, including multiple infrared active vibrant bonds, such as the stretching vibration and bending vibration of Si-O-Si band in the [SiO_4] tetrahedron, the O-H band in hydroxyl and the other bands of metal ions with oxygen. The unique elements and structure of tourmaline cause its high irradiating far-infrared radio reaching to 0.90, and the wavelength range is 4-14 μm [21]. Tourmaline could radio far-infrared, which activate the intramolecular and intermolecular vibrations to diminish the clusters of water molecules and promote ionization of H_2O, therefore the intermolecular forces of water is reduced [26,27]. Thus the higher electrical conductivity and lower surface tension were detected.

3.2 XRD characterization

XRD characterization was investigated for the phase structure and phase composition of A-F photocatalyst samples (Fig. 1). It was indicated that, the pure TiO_2 particles as the control (Sample A) exhibited well crystallized phases of anatase (JCPDS No. 21-1272) and rutile (JCPDS No. 21-1276). The Sample B photocatalyst also had both anatase and rutile phases, wherein the rutile phase with growth trend. The Sample D photocatalyst had larger proportion of anatase phase than other samples. The Sample C, E and F photocatalysts had anatase as the main phase. However, no tourmaline structure (2θ values=22.28, 30.28, and 34.78, JCPDS. No. 43-1464) was found because of the limit amount below the detectable. From Fig. 1, it was also noteworthy that no peaks corresponding to CeO_2 was observed in each doped TiO_2 samples (Sample B, D, E and F). According to the literatures [18,19 and 31], one reason was that the concentration of dopant Ce was too low to be detected via XRD. The other was that the ionic radius of Ce^{4+} (0.092 nm) was much larger than that of Ti^{4+} (0.065 nm), it was

Table 2 The electrical conductivity and surface tension of deionized water effected via tourmaline

Time (min)	Electrical conductivity of deionized water (μs/cm)		Surface tension of deionized water (mN/m)	
	With tourmaline	Without tourmaline	With tourmaline	Without tourmaline
0	1.56±0.01	1.56±0.01	71.69±0.06	71.69±0.06
30	1.81±0.01	1.58±0.02	64.53±0.06	72.35±0.04
60	1.94±0.02	1.59±0.03	64.87±0.03	71.77±0.05
90	2.02±0.03	1.57±0.02	65.25±0.02	72.14±0.03
120	2.07±0.02	1.58±0.02	64.54±0.04	71.84±0.02

hard to achieve the substitution of Ce^{4+} for Ti^{4+} in composite photocatalysts. By comparison, there was no peak shift phenomenon and change of the lattice constants between B, D, E, F and A samples, indicating that Ce (0.102 nm) elements were not incorporated into the structure of TiO_2. Therefore, Ce existed as the forms of uniformly dispersed small cluster CeO_2 onto the surface or interstitial site of TiO_2.

The 2θ values of 25.38, 37.88, and 48.18 corresponded to the crystal planes of (101), (004), and (200) of the anatase TiO_2 phase, respectively. With regard to Sample C, D, E and F, the peak widths were broadened and indicated smaller crystallite sizes compared with Sample A. Because the component tourmaline has the spontaneous polarization property, it could be seen as a pair of electric dipole, the two ends of tourmaline particles equate to the positive and negative poles of the electric field (shown as Scheme 1). During the preparation of C, E and F photocatalysts, the monomers formed sol particles trough hydrolysis and condensation reactions. The ion particles $[Ti(OR)_4(H_3O)_n^{n+}]$ charged positive in sol were attracted by the negative electrode of tourmaline particles, and Cl^- attracted via the positive electrode. Furthermore, the electric field and high far-infrared radiation [21] of tourmaline particles could activate the vibrations of water molecules and diminish the clusters of water molecules, providing high conductivity and low surface tension of water (Table 2) as above discussion. The sol particles aggregated and grew via the electric field attraction of tourmaline, thus more and more crystal nucleus was formed around tourmaline. Therefore, the ions moved more rapidly and sol particles grew faster than the control TiO_2 sample, and the spatial effect made the smaller crystallite particle sizes. It was assumed that, the small size of single particles would reduce the backlog inside the lattice, and the far infrared of tourmaline could strengthen bond vibration, therefore the bond distance of Ti-Ti trends to larger to form anatase phase (0.304~0.379 nm) instead of rutile phase (0.195~0.198 nm). Moreover, CH_3COOH acted on the nonhydrolytic processing of the [001]-oriented and the form of anatase crystal, which could be promoted by the electric field and high far-infrared radiation of tourmaline particles for the stability of anatase crystalline-phase [32,33]. The Sample C, E and F photocatalysts including tourmaline facilitated anatase as the main phase. During the preparation of Sample B, tourmaline particles were absent and cerous nitrate solution was dropped in to the solution before HCl and CH_3COOH were added. Ce^{3+} as foreign ions might disturb the form of normal sol, therefore the form of sol particles was not perfect and uniform, and rutile phase appeared. During the preparation of Sample D, tourmaline particles and cerous nitrate solution were dropped in to the solution before HCl and CH_3COOH were added. The electric field and high far-infrared radiation of tourmaline, besides foreign ion Ce^{3+} might disturb the form of normal sol, therefore the form of sol particles was not perfect and uniform, and more rutile phase appeared compared with C, E and F. It was exposed that, the addition sequence of Ce and tourmaline could affect the phases and particle size of composite photocatalysts.

3.3 Microstructure characterization

Fig. 2 showed the SEM and TEM photographs of Sample A-F photocatalytic films. In the SEM morphologies it is shown that, the D_{50} of tourmaline was 0.40 μm, and the diameter of pure TiO_2 particles in Sample A was around 150 nm. The nanoparticles of Sample B, C, D, E and F films were smaller than pure TiO_2 particles of Sample A and got larger surface area, which was consistent to the results of XRD characterization and TEM images of Sample B and F. In Sample C, E and F films, tourmaline particles were wrapped up by nanoparticles, which formed nanoparticles clusters and higher surface area (Fig. 2C, E, F and I). In Sample B film, compared with Sample A, smaller nanoparticles (Fig. 2B and H) formed the cascade distribution and rough surface, which also made higher surface area. The SEM photographs showed both Ce and tourmaline made the diameters of TiO_2 particles smaller than that of pure TiO_2 sample, therefore Sample B, C, D, E and F photocatalytic films had higher surface area than the control sample TiO_2 film (from 23.82 m^2/g rise to about 40 m^2/g, Table 3). It was shown that, the addition of Ce and tourmaline affect the microstructure of TiO_2 nanoparticles.

Through EDS analysis it was known: In Sample C film, the nanoparticles around clusters only contained Ti, O, and Cl elements, part of TiO_2, wherein the Cl elements from HCl of the titanium sol. The nanoparticles of the clusters contained not only Ti, O, and Cl elements, but also Fe, Al, Si, Ca, K, Mg elements, which belong to tourmaline. It was illustrated that, the tourmaline particles were wrapped up via TiO_2 nanoparticles. In addition, Sample E and F films had the similar conclusion: tourmaline particles were wrapped up via Ce-doped TiO_2 nanoparticles. Combining the results of XRD characterization, the SEM and TEM photographs confirmed the microstructure of Sample F and its synthetic route (shown as

Table 3 The specific surface areas and pH values during MO degradation reaction of Sample A-F

Sample	S_{BET} (m^2/g)	pH values for MO degradation reaction at interval time			
		0 h	1 h	2 h	3 h
A	23.82	5.23	5.29	5.18	5.17
B	38.26	5.26	5.25	5.19	5.16
C	39.88	5.23	5.15	5.21	5.19
D	39.75	5.28	5.18	5.17	5.21
E	40.65	5.30	5.21	5.18	5.18
F	41.23	5.18	5.13	5.15	5.18

Scheme 1). In Sample D film, the tourmaline particles were added before titanium sol, and might disturb the prime of sol particle nucleus, so the photocatalyst nanoparticles were not wrapped around the tourmaline perfectly, which was in accordance with the discussion of XRD results as above.

3.4 UV-vis diffuse reflectance spectra of different composite photocatalyst

The absorption edge of the Sample A-F composites is shown in Fig. 3. Compared with Sample A and Sample C (without doping Ce), it is revealed that Sample B, D, E and F have a light absorption in range of 400-500 nm (visible light portion), because of doping with Ce to narrow the band gap of TiO_2 composite photocatalysts. However, the low doping content of Ce induced the low absorption of visible light. In consideration of the increased absorption of UV light, the UV light (253.7 nm) was still used as a light source for the photodegradation of MO.

3.5 Photocatalytic activity to methyl orange of different composite photocatalysts

Fig. 4 shows the photocatalytic degradation of MO via stainless steel net surface plated with Sample A-F films. With regard to TiO_2 composite films, the content of tourmaline was 0.40 wt% and the content of Ce was 0.10 wt%. The degradation time was 180 min, and MO decolorization ratio increased significantly with the increase of reaction time. It was known from Fig. 3, the TiO_2 film photocatalytic degradation ratio of MO was the lowest 59.0%, Sample B film was 68.3%, Sample C, D and E films were all around 83%, Sample F film was up to 94.6%. It was shown that, the photocatalytic efficiency of TiO_2 composite photocatalysts could be improved via tourmaline or rare earth. And the efficiency of MO photocatalytic degradation via Sample F composite film was higher than both Sample B and C. This conclusion was confirmed by the optical images of MO photodegradation in Fig. 5.

Among these samples with different composites and preparation process, Sample F had the highest photocatalytic efficiency. Tourmaline was a unique polar mineral and tourmaline particles can be seen as many individual micro-electrical fields. During preparing Sample F as shown in Scheme 1, the anode electric field of tourmaline particles weakened the adsorption of titanium ions, which stopped the crystal growing and formed the titanium crystal with smaller size. This morphology provides the larger specific surface for much more photocatalytic active sites, so that the composite photocatalyst system can more fully contact with the reactant, increase the utilization rate of reaction activity point. During the photocatalyst reaction as shown in Scheme 2, TiO_2 was excited by the light energy greater than the band gap, electrons of the valence band jumped across the band gap into the conduction band, and left a hole in the valence band. The photogenerated electrons reacted with O_2 dissolved in the water to form superoxide radical (O_2^-); Hydroxyl (OH^-) trapped photogenerated holes to produce hydroxyl radical (·OH), hydroxyl radical can take hydrogen abstraction reaction with organic pollutants. The strong oxidation ability of O_2^- and ·OH free radicals colud degrade MO. However, during electron transition from the valence band to the conduction band, there will be a considerable part of the photogenerated electrons accelerated to the valence band and recombine with holes. Cerium doped in the experiment and existed as the tetravalent cerium state because of easily oxidization at high temperature, equivalent to narrow the band gap in titanium dioxide, which can expand the spectral response range to improve the photocatalytic efficiency. In addition, the tourmaline particle with its own permanent electrode, can be seen as a pair of electric dipole, according to the following formula: $Er=(2/3)E_0(a/r)^3$ (where a is a tourmaline particle radius, r is the distance from the center). According to our previous study [21], the electric field is about 10^4 ~ 10^7 (the highest value) V/m in the ten micron range of tourmaline surface, which promoted the generation of OH^- from H_2O and the MO adsorption onto the surface of catalysts. The photocatalyst nanoparticles were excited to generated electrons and holes by the irradiation of UV, thus the photogenerated electrons were also adsorbed on the anode of tourmaline particles to form O_2^- and avoid the recombination of photogenerated electron-holes, which also improve the utilization rate of photogenerated holes. At the same time, the infrared ray of tourmaline particles can enhance the molecular motions and promote the decrease of water molecules cluster $(H_2O)_n$, to improve the solubility of O_2, which is conducive to organic pollutants degradation reaction. The natural electric field and radiation of far infrared ray from tourmaline particles, and the reaction of rare earth element Ce, jointly effect on TiO_2 photocatalytic degradation of organic pollutants.

The pH value for MO degradation reaction of every sample was detected as Table 3. It is known that the pH values for every reaction is kept around 5.2, no obvious changes has been shown. As acetic acid was used for the preparation of each sample (seen as Table 1), the acidity of reaction solutions (pH=5.2~5.3) appeared at the beginning (at 0 h), which is beneficial to MO degradation of all the samples. During MO degradation, Ce could promote the photogeneration electron-hole pairs, and the tourmaline could promote the ionization of H_2O to form H^+ and OH^-. Thus the protons promoted by Ce and tourmaline would rapidly form radicals with high reactivity such as OH radicals (shown as Fig. 6), be utilized to degrade MO. Therefore, pH value is kept around 5.2, and the MO degradation accelerated by more radicals during reaction.

According to the other researchers' literatures [23,34], the rutile phase of TiO_2 had lower photocatalytic activity than the anatase phase, but the anatase and rutile phases of mixed-phase TiO_2 had higher photocatalytic activity than pure phase TiO_2. However, the synergistic effect of tourmaline and rare earth made great enhancement of TiO_2 photocatalytic activity, compared with the control TiO_2 sample with the anatase and rutile mixed-phase. Therefore, the best photocatalytic activity got following the preparation process of Sample F.

As the relevant literatures [17,18], cerium doped was introduced into Sample B film as Ce^{3+} (cerium nitrate). Because of the high temperature, the Ce^{3+} is easily oxidized and existed in the form of Ce^{4+}, which formed the CeO_2-TiO_2 system in the film, and could narrow the band gap of the photocatalyst to make the excitation of photogenerated-electronFs easy [35].

Furthermore, the smaller size of photocatalyst nanopaticles had more surface area and active sites, which improved the photocatalytic efficiency of Sample B (68.3%) compared with TiO_2 (59.0%). In Sample C, D and E films, the photocatalytic degradation ratio of MO were all around 83% for 3 h. As sapmle C composite film similar to the photocatalyst studied previous [21], tourmaline was a unique polar mineral and formed the titanium crystal with smaller size to increase photocatalytic surface area. Furthermore, tourmaline could hinder the recombination of photogenerated electron-hole from TiO_2, and enhance the photocatalytic activity. During the preparation of Sample D and E, cerous nitrate solution and tourmaline were added together before or after the form of titanium sol, tourmaline might disturbe the form of uniform sol particles with Ce. Therefore, Sample C, D, E films had improved the photocatalytic activity, but did not get the highest photocatalytic activity because of the disturbance between Ce and tourmaline during the preparation. Therefore, the addition sequence of preparation process could effect on the photocatalytic activity of TiO_2 composite photocatalyst.

3.6 Effect of tourmaline content on the photocatalytic activity

In consideration of Sample F possessing the highest photocatalytic activity as section 3.5 discussed, the optimal contents of tourmaline for this composite photocatalyst sample were detected. As is seen from Fig. 7, in the same light conditions and photocatalytic time, the composite photocatalyst samples (follow the preparation process of Sample F) comprising the different contents of tourmaline (0 wt%, 0.20 wt%, 0.40 wt% and 0.60 wt%, respectively) performed different photocatalytic activities. The activities of MO photocatalytic degradation via samples with tourmaline were stronger than the sample without tourmaline (Sample B). Moreover, the mass fraction with 0.40 wt% had the strongest catalytic degradation activity of MO (within 3 h, the photocatalytic degradation ratio of MO reached 94.6%). Thus with the increase of mass fraction of tourmaline, the MO photocatalytic degradation of Sample F declined.

The reason of this trend is: when the tourmaline content was too small, it was difficult to form activity center; as reaching a moderate amount, tourmaline could effectively control the TiO_2 grain growth in crystals, and reduce the recombination rate of electron and hole, so that the TiO_2 composite catalyst produced more ·OH to improve the activity of the catalyst. However, the high content of tourmaline would adsorb excessive photogenerated electrons and reduce O^{2-} content, thus affected the photocatalytic activity. If the tourmaline mass fraction continues to increase, tourmaline will package on the TiO_2 surface, which leads to decrease the photocatalytic activity centers and reduce the photocatalytic degradation activity. Moreover, immoderate addition of tourmaline would disturb the preparation of film on stainless steel meshes. Therefore, 0.40 wt% was the addition of tourmaline for Sample F.

3.7 Effect of Ce content on the photocatalytic activity

As is seen from Fig. 8, in the same light conditions and photocatalytic time, the composite photocatalyst samples (follow the preparation process of Sample F) comprising different contents of Ce (0 wt%, 0.05 wt%, 0.10 wt% and 0.15 wt%, respectively) performed different photocatalytic activities. In 3 h, the MO photocatalytic degradation ratios of samples with different Ce content were 68.3%, 90.0%. 94.6% and 88.9%, respectively. Among these samples, the film with 0.10% of Ce content (the same as Sample F of section 3.5 discussed) had the highest ratio of photocatalytic degradation. When Ce content increased to 0.15%, the photocatalytic activity began to slow down. It means that, too much or too little content of Ce was not conducive to improve the photocatalytic activity of composite photocatalyst sample. In the heating case of preparation, Ce^{4+} will gradually migrate from anatase phase to the TiO_2 powder surface. Under UV light, Ce^{4+} also could generate electron-holes, therefore doped rare earth compound could increase the catalyst activity. But the excess dopant would make the rare earth ion deposited on TiO_2 surface to form the composite center of charge carriers, thus lowering the photocatalytic activity. Therefore, 0.10 wt% was the appropriate addition of Ce for Sample F.

Through the XRD and SEM characterization, our study inferred that the addition sequence of Ce and tourmaline effected on the microstructure of TiO_2 composite photocatalysts. As Sample F, Ce was added before primary titanium sol, which could dispersed uniformly with primary titanium solution and not disturb the formation of sol nucleus around tourmaline. Movemore, tourmaline particles were added after primary titanium sol, and made smaller size of TiO_2 nanoparticles, higher surface area and more activity sites. By means of MO photocatalytic degradation ratio, it was revealed that the microstructure could enhance the photocatalytic activity; meanwhile, doped Ce narrowed the band gap, tourmaline hindered the recombination of photogenerated electron-hole and promoted the oxidative degradation of MO. Because of the synergy-effect of Ce and tourmaline on the microstructure and photocatalytic activity of TiO_2 composite photocatalyst, Sample F with 0.10 wt% Ce and 0.40 wt% tourmaline had the highest MO photocatalytic degradation ratio.

Conclusions

During the preparation of TiO_2 composite photocatalyst, tourmaline particles as many individual micro-electrical fields, could restrict the crystal growing and form smaller titanium nanoparticles. This concave convex morphology was significant for increasing the surface areas and active sites to improve the photocatalytic efficiency. Besides, the electrostatic adherence and physical adsorption of tourmaline were also conducive to the contact between organic pollutants and active sites. In the electric field of tourmaline, the photogenerated electrons were adsorbed on the anode of tourmaline, further avoiding the recombination of photogenerated electrons and holes. In the comprehensive effect of far infrared and electric field of tourmaline, the ionization process of water has accelerated, is conducive to the formation of hydroxyl radicals, thus improving the photocatalytic activity. Furthermore, Ce

narrowed the band gap of TiO_2 composite photocatalyst, which also enhance the degradation reaction of organic pollutants.

This paper prepared tourmaline, Ce and TiO_2 composite photocatalysts via a sol-gel method. Through detecting the photocatalytic activity of the composite photocatalysts with different preparation methods and component contents, and analyzing the effect of tourmaline and Ce on the composite catalyst, we took a preliminary study on the synergy mechanism of tourmaline and Ce on TiO_2 composite photocatalyst and summarized the appropriate preparation process and component proportion (Sample F with 0.10 wt% Ce and 0.40 wt% tourmaline). This study has provided the preparation of TiO_2 photocatalyst improved with Ce and tourmaline, which is a green and promising technique in organic pollutants degradation and environmental protection area.

Acknowledgements

This project was supported by Leading Talent Cultivation Plan for Hebei Province Higher Education Innovation Team of China (Grant NO. LJRC020).

Notes and references

1 M. A. Ahmed, *J. Photoch. Photobio. A,* 2010, **238**, 63.
2 P. Gao, J. Liu and T. Zhang, *J. Hazard. Mater.,* 2012, **229-230**, 209.
3 Y. Xie, Q. N. Zhao and X. J. Zhao, *Catal. Lett.,* 2007, **118**, 231.
4 X. Feng, K. Shankar and O.K. Varghese, *Nano Lett.,* 2008, **8**, 3781.
5 Z. Lai, F. Peng and Y. Wang, *J. Mater. Chem.,* 2012, **22**, 2390.
6 Z. Hu, J. C. Yu, *J. Mater. Chem. A*, 2013, **1**, 12221.
7 Z. Hu, J. C. Yu and T. Ming, *Appl. Catal. B,* 2015, **168-169**, 483.
8 C. B. Zhang, H. He and K. Tanaka, *Appl. Catal. B,* 2006, **65**, 37.
9 S. Sun, J. J. Ding and J. Bao, *Appl. Surf. Sci.*, 2012, **258**, 5031.
10 T. Nogawa, T. Isobe and S. Matsushita, *Mater. Lett.,* 2012, **82**, 174.
11 Q. R. Deng, X. H. Xia and M. L. Guo, *Mater. Lett.,* 2011, **65**, 2051.
12 Y. H. Liu, Z. L. Wang and W. B. Fan, *Ceram. Int.,* 2014, **40**, 3887.
13 H. Y. Wei, Y. S. Wu and N. Lun, *J. Mater. Sci.,* 2004, **39**, 1305.
14 F. B. Li, X. Z. Li and C. H. Ao, *Chemosphere*, 2005, **59**, 787.
15 T. Z. Tong, J. L. Zhang and B. Z. Tian, *J. Colloid. Interf. Sci*, 2007, **315**, 382.
16 S. Kityakarn, Y. Pooarporn and P. Songsiriritthigul, *Electrochim. Acta*, 2012, **83**, 113.
17 S. N. R. Inturi, T. Boningari and M. Suidan, *Appl. Catal. B,* 2014, **144** , 333.
18 A. Charanpahari, S. S. Umare and R. Sasikala, *Appl. Surf. Sci*, 2013, 282, 408.
19 Z. H. Meng, L. H. Wan and L. J. Zhang, *J. Ind. Eng. Chem.*, 2014, **20**, 4102.
20 X. G. Sun, C. M. Li and L. Y. Ruan, *J. Alloy. Comp.*, 2014, **585**, 800.
21 J. S. Liang, J. P. Meng and G. C. Liang, *T. Nonferr. Metal. Soc.*, 2006, **16**, s542.
22 S. H. Song and M. Kang, *J. Ind. Eng. Chem.*, 2008, **14**, 785.
23 G. K. Zhang and X. Qin, *Mater. Res. Bull.*, 2013, **48**, 3743.
24 Z. Wu, H. Wang and K. Zheng, *J. Phys. Chem. C*, 2012, **116**, 12814.
25 R. R. Yeredla and H. Xu, *J. Phys. Chem. C*, 2008, **112**, 532.
26 Donnay. G, *Acta Crystallogr.*, 1977, **A33**, 927.
27 Nakamura T, Kubo T. *Ferroelectrics*, 1992, **137**, 13.
28 Z. Shen, S. Sun and W. Wang, *J. Mater. Chem. A*, 2015, **3**, 3285.
29 F. Wang, Wilson Kwok Hung Ng and J. C. Yu, *Appl. Catal. B*, 2012, **111-112**, 409.
30 K. Ishibashi, A. Fujishima and T. Watanabe, *Electrochem. Commun.*, 2000, **2**, 207.
31 X. Cao, D. Li and W. Jing, *J. Mater. Chem.,* 2012, **22**, 15309.
32 J. F. Ye, W. Liu and J. G. Cai, *J. Am. Chem. Soc.*, 2011, **133**, 933.
33 P. Gao, A. R. Li and D. D. Sun, *J. Hazard. Mater.*, 2014, **279**, 96.
34 Y. L. Zhang, H. H. Gan and G. K. Zhang, *Chem. Eng. J.*, 2011, **172**, 936.
35 J. H. Park, W. S. Kim and D. H. Jo, *J. Ind. Eng. Chem.*, 2014, **20**, 1965.

Figure Captions

Scheme 1. Synthetic route of Sample F photocatalyst nanoparticles

Scheme 2. Synergistic effects of tourmaline and Ce on MO photocatalytic degradation of TiO_2 composite photocatalyst (Sample F)

Fig. 1 XRD patterns of photocatalyst Sample A-F (the details of every sample were listed as Table 1)

Fig. 2 SEM (A: Sample A photocatalyst; B: Sample B photocatalyst; C: Sample C photocatalyst; D: Sample D photocatalyst; E: Sample E photocatalyst; F: Sample F photocatalyst; G: Tourmaline particles) and TEM (H: Sample C photocatalyst; I: Sample F photocatalyst) photographs of the tourmaline and different photocatalyst samples

Fig. 3 UV-vis diffuse reflectance spectra of Sample A-F photocatalysts

Fig. 4 The MO photocatalytic degradation ratio of Sample A-F photocatalysts

Fig. 5 The optical images of MO photodegradation by Sample A-F under UV light after different times (0 h and 3 h)

Fig. 6 The fluorescence spectra for OH radicals of Sample A-F in the terephthalic acid solution (after 30 min of UV light illumination)

Fig. 7 The degradation ratio of MO by composite photocatalyst samples with different tourmaline contents (0 wt%; 0.20 wt%; 0.40 wt%; 0.60 wt%)

Fig. 8 The degradation ratio of MO by composite photocatalyst samples with different Ce contents (0 wt%; 0.05 wt%; 0.10 wt%; 0.15 wt%)

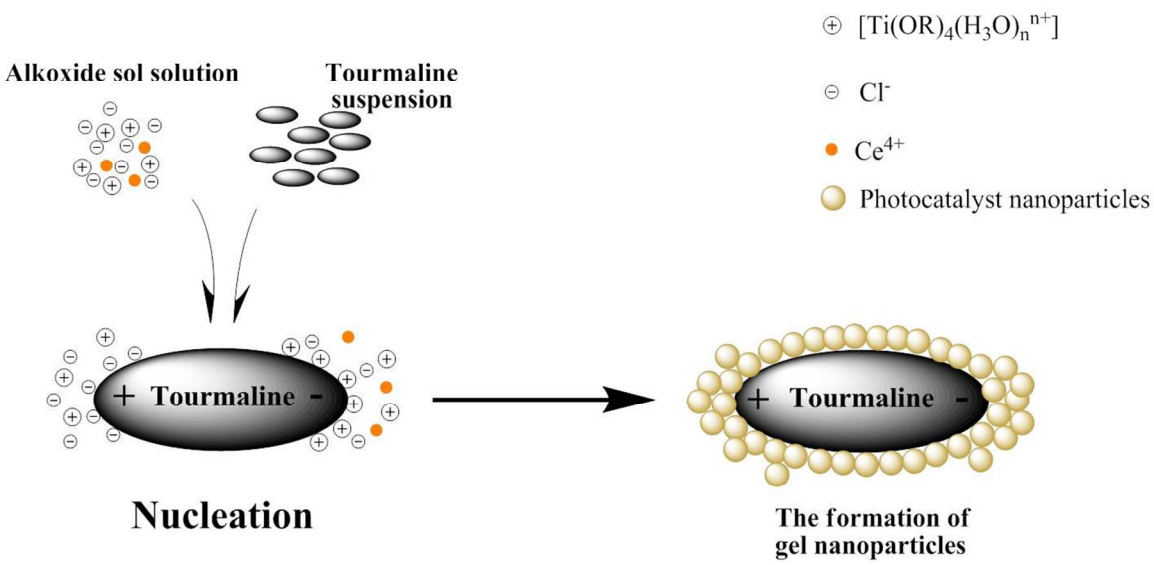

Scheme 1. Synthetic route of Sample F photocatalyst nanoparticles

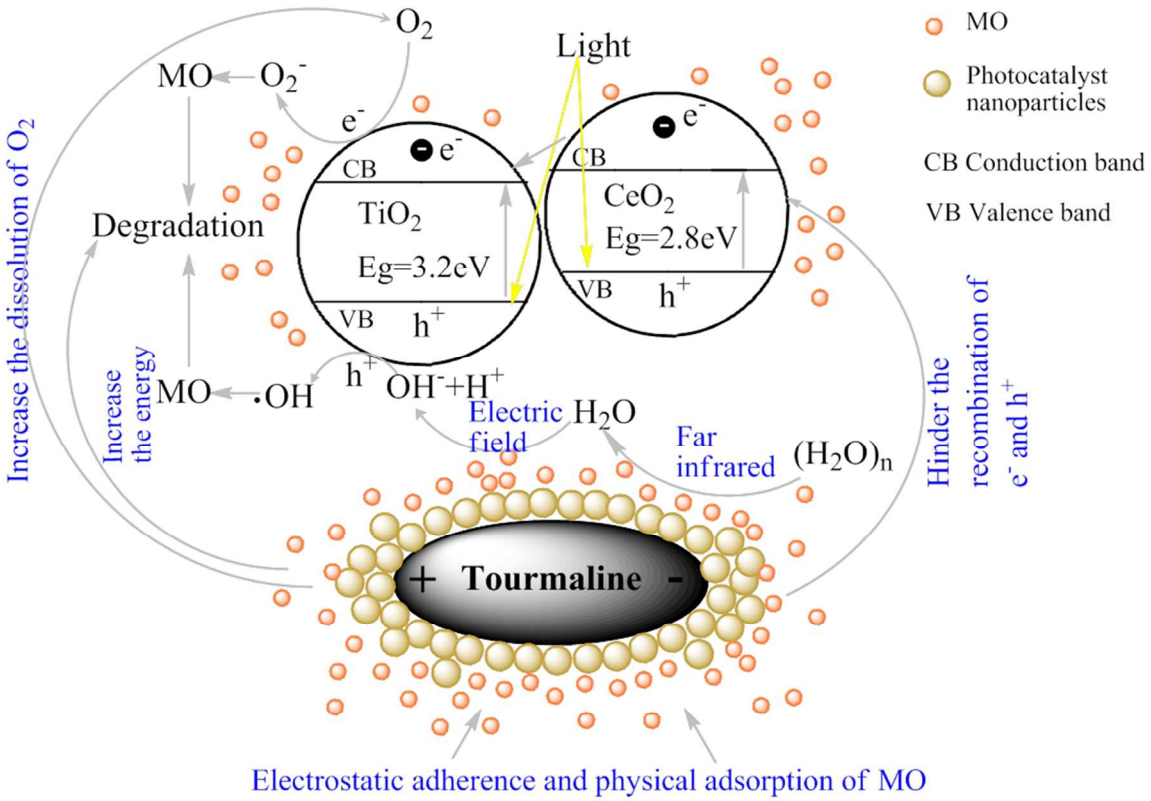

Scheme 2. Synergistic effects of tourmaline and Ce on MO photocatalytic degradation of TiO_2 composite photocatalyst (Sample F)

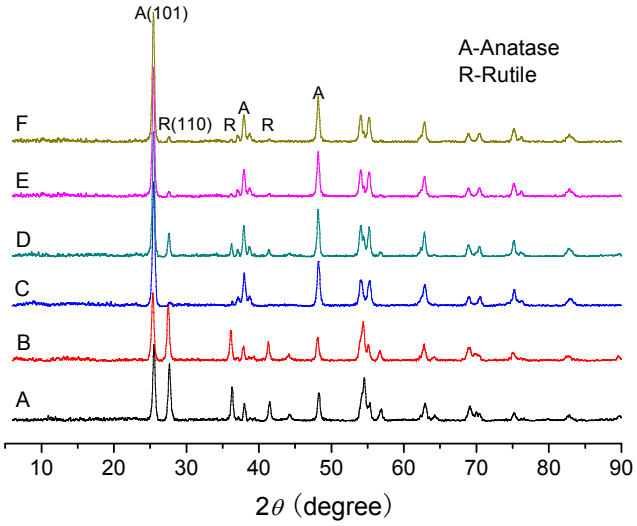

Fig. 1 XRD patterns of photocatalyst Sample A-F (the details of every sample were listed as Table 1)

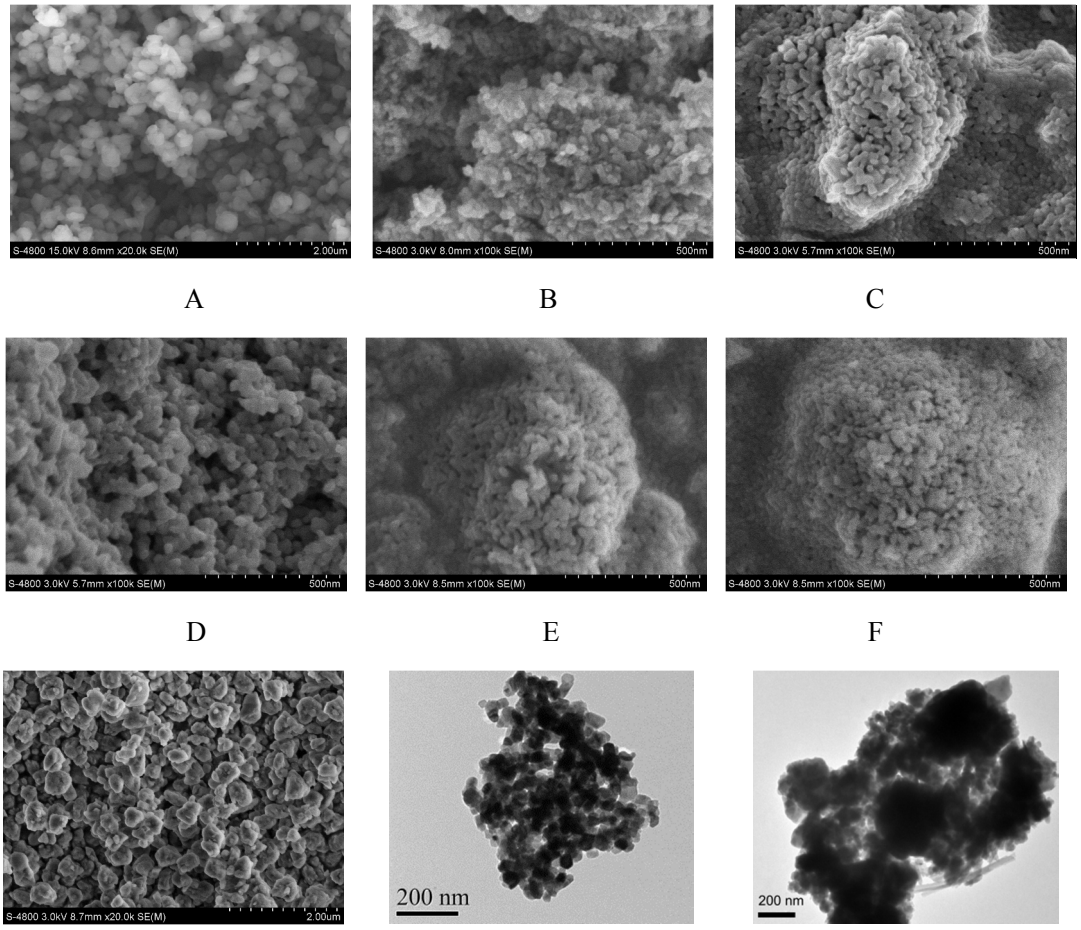

Fig. 2 SEM (A: Sample A photocatalyst; B: Sample B photocatalyst; C: Sample C photocatalyst; D: Sample D photocatalyst; E: Sample E photocatalyst; F: Sample F photocatalyst; G: Tourmaline particles) and TEM (H: Sample C photocatalyst; I: Sample F photocatalyst) photographs of the tourmaline and different photocatalyst samples

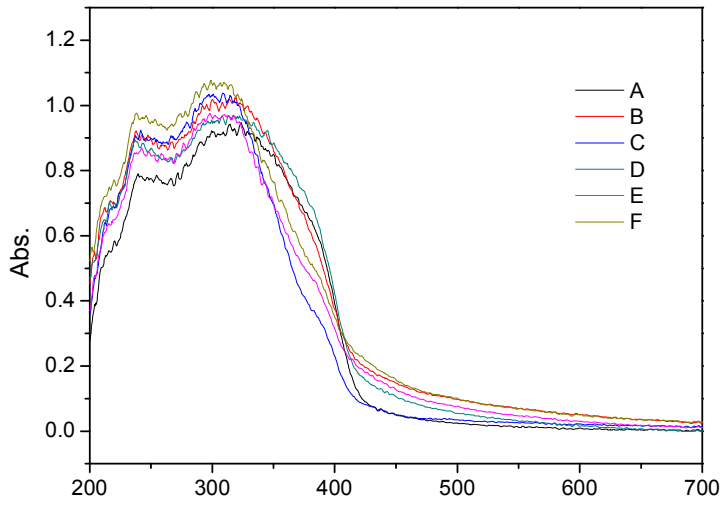

Fig. 3 UV-vis diffuse reflectance spectra of Sample A-F photocatalysts

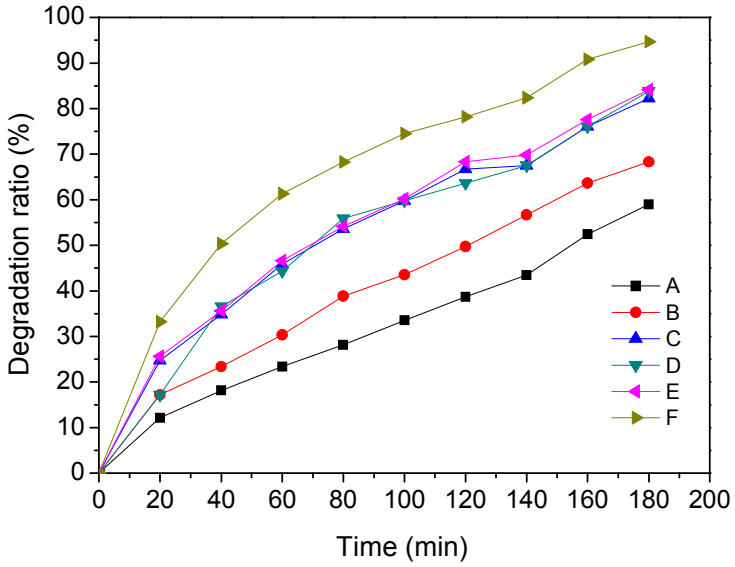

Fig. 4 The MO photocatalytic degradation ratio of Sample A-F photocatalysts

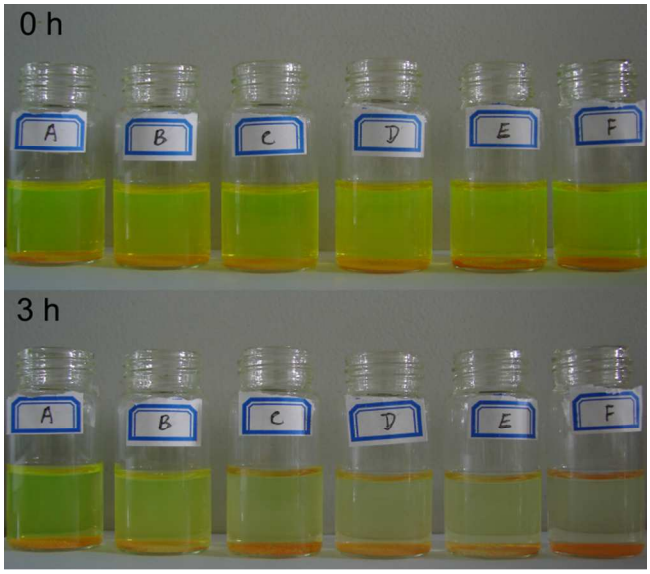

Fig. 5 The optical images of MO photodegradation by Sample A-F under UV light after different times (0 h and 3 h)

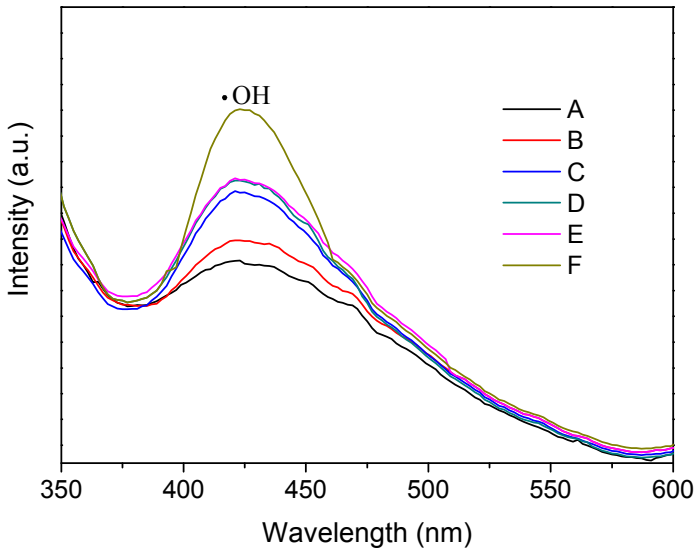

Fig. 6 The fluorescence spectra for OH radicals of Sample A-F in the terephthalic acid solution (after 30 min of UV light illumination)

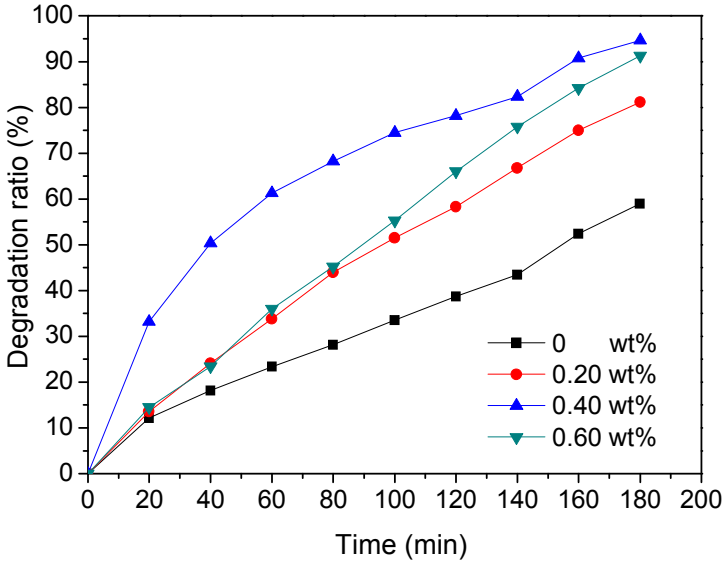

Fig. 7 The degradation ratio of MO by composite photocatalyst samples with different tourmaline contents (0 wt%; 0.20 wt%; 0.40 wt%; 0.60 wt%)

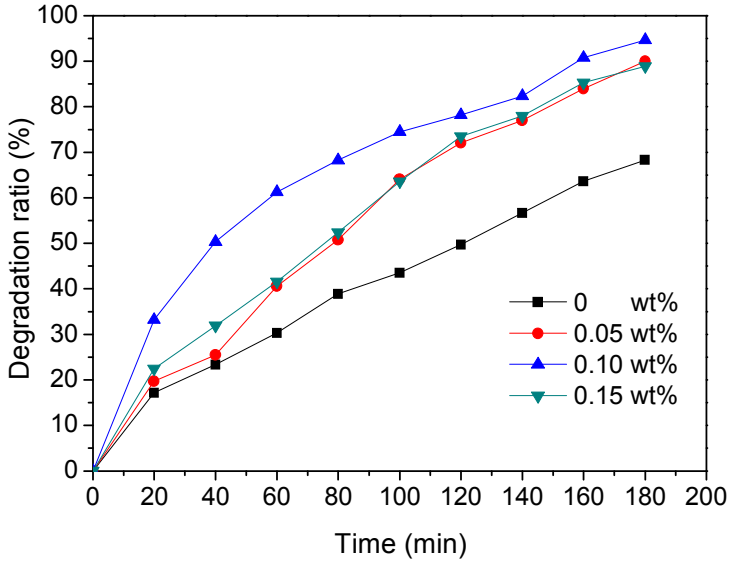

Fig. 8 The degradation ratio of MO by composite photocatalyst samples with different Ce contents (0 wt%; 0.05 wt%; 0.10 wt%; 0.15 wt%)